Published in final edited form as:
Microcirculation. 2012 October ; 19(7): 619–631. doi:10.1111/j.1549-8719.2012.00197.x.

Laser Speckle Flowmetry Method for Measuring Spatial and Temporal Hemodynamic Alterations Throughout Large Microvascular Networks

Joshua K. Meisner[1], **Suna Sumer**[1], **Kelsey P. Murrell**[1], **Timothy J. Higgins**[1], and **Richard J. Price**[1,2]

[1]Department of Biomedical Engineering, University of Virginia, Charlottesville, Virginia, USA

[2]Departments of Radiology and Radiation Oncology, University of Virginia, Charlottesville, Virginia, USA

Abstract

Objectives—1) Develop and validate laser speckle flowmetry (LSF) as a quantitative tool for individual microvessel hemodynamics in large networks. 2) Use LSF to determine if structural differences in the dorsal skinfold microcirculation (DSFWC) of C57BL/6 and BALB/c mice impart differential network hemodynamic responses to occlusion.

Methods—We compared LSF velocity measurements to known/measured velocities in vitro using capillary tube tissue phantoms and in vivo using mouse DSFWCs and cremaster muscles. Hemodynamic changes induced by feed arteriole occlusion were measured using LSF in DSFWCs implanted on C57BL/6 and BALB/c.

Results—In vitro, we found that the normalized speckle intensity (NSI) versus velocity linear relationship ($R^2 \geq 0.97$) did not vary with diameter or hematocrit and can be shifted to meet an expected operating range. In vivo, DSFWC and cremaster muscle preparations ($R^2=0.92$ and 0.95, respectively) demonstrated similar linear relationships between NSI and centerline velocity. Stratification of arterioles into predicted collateral pathways revealed significant differences between C57BL/6 and BALB/c strains in response to feed arteriole occlusion.

Conclusions—These data demonstrate the applicability of LSF to intravital microscopy microcirculation preparations for determining both relative and absolute hemodynamics on a network-wide scale while maintaining the resolution of individual microvessels.

Keywords

laser speckle flowmetry; hemodynamics; network blood flow; intravital microscopy; microvascular imaging

Introduction

The proper maintenance of microvascular network structure and vasoactivity is essential for normal tissue physiology and function both in the short term (i.e. via smooth muscle tone) and long term (i.e. via remodeling of vascular wall structure) (34). Vascular wall shear stress is generally thought to play a central role in coordinating the sequence of events leading to arteriolar remodeling (28, 34, 35). However, few studies are aimed at determining the

---

Corresponding Author: Richard J. Price, University of Virginia, Department of Biomedical Engineering, Room 2316 MR5 Building, Charlottesville, Virginia, 22903, rprice@virginia.edu.

molecular mechanisms of coordinated arteriolar remodeling in response to shear stress, even in light of its clinical significance to hypertension, peripheral arterial disease, tumor vascularization, and retinopathy. One major reason for why mechanistic investigation in this important field has been limited is that experimental approaches capable of quantitatively linking shear stress changes to arteriolar remodeling in individual vessels over time throughout large microvascular networks are widely unavailable, limiting many of the few existing studies to computational approaches or single time points (35, 36). Here, we define a network as the interconnected structure of all microvessels from feeding arterioles to draining venules in the visible microvascular preparation.

One potential method for quantitatively measuring network autoregulation is laser speckle flowmetry (LSF). Laser speckle imaging works on the principle that coherent light (i.e. laser light) creates a random interference (speckle) pattern when shone on a static tissue region, with reduced contrast in regions exhibiting motion. Initially proposed in 1981, Fercher and Briers (19) showed that, using spatial statistics, it is theoretically possible to create a 2-dimensional distribution map of velocity based on the dynamic motion of scattering particles in a tissue (see reviews (7, 16)). With the technological advances in CCD and CMOS cameras, as well as improvements in statistical algorithms for enhanced temporal and spatial resolution (11, 16, 37) and processing power (48), the LSF technique has become readily accessible with a demonstrable ability to produce distribution maps of blood flow in the microcirculation (e.g. pial circulation (2, 3, 18, 44), mesentery (10), dorsal skinfold window chamber (12, 37, 47) and retina (29)). Therefore, LSF presents a clear opportunity to quantify hemodynamics at the resolution of the microcirculation.

To date, however, laser speckle imaging has been largely limited to use as a qualitative tool of regional perfusion (2, 3, 16, 18, 44), even when correlated to microvascular remodeling (38). One of the key factors leading to this limitation in current applications is the use of low-magnification optical components that are needed to capture an entire network within a single field of view. This limits the ability to resolve the majority of components of the microcirculation. This limitation has been historically overcome using intravital microscopy techniques in two-dimensional networks to observe the microcirculation at high magnification. A second key issue is that, of the few studies specifically suggesting the potential of laser speckle imaging in the microcirculation (10, 16, 47), there has been a lack of validation in vivo, which is of particular concern given the debated quantitative potential of speckle in vivo (see review (17)). Therefore, we tested and validated the use of LSF with intravital microscopy of the mouse cremaster muscle and dorsal skinfold window chamber using particle imaging velocimetry of circulating fluorescent microspheres. Subsequently, we sought to demonstrate the potential of LSF toward quantifying changes in hemodynamics throughout the dorsal skinfold window chamber. Specifically, the potential of LSF to quantify network hemodynamics was applied to test how strains known to have large differences in microvascular network structure (i.e. C57BL/6 and BALB/c (21, 40, 49)) acutely respond to changes in network flow.

Method and Materials

Animals

All animal studies were approved by the Animal Research Committee at the University of Virginia and conformed to the AHA Guidelines for the Use of Animals in Research. C57BL/6 and BALB/c male mice, 8–10 weeks of age, were purchased from Charles River Laboratories (Wilmington, MA). “n” values for each experiment are provided in the figure legends.

Dorsal Skinfold Window Chamber Implantation for Intravital Imaging

Window chamber surgeries were performed in a similar procedure to that previously described by our laboratory (33). Briefly, wild type mice were anesthetized by i.p. injection of ketamine, xylazine, atropine, and saline (100/20/0.4 mg/g body weight), with supplemental doses equal to one fifth of the initial dose administered as required. After anesthesia, the dorsal skin was depilated and sterilized. Using a dissecting microscope, one half of a dorsal skinfold window chamber was surgically attached. A 12mm diameter circular section of the entire top skin tissue layer and subcutaneous tissue was excised under sterile conditions to expose the microcirculation of the underside of the dermis in the opposite layer skin with a goal of minimizing damage to the microvascular network. The second half of the window chamber was installed, and the exposed network was filled with sterile Ringer's solution and covered with a sterile glass coverslip that inserts into the titanium frame. Buprenorphine was administered by subcutaneous injection post-operatively for analgesia (0.3mg/g body weight). After the end of the experiment, the mouse was euthanized with an overdose of pentobarbital.

Cremaster Muscle Preparation for Intravital Imaging

The cremaster muscle was isolated similar to a previously described method (4). Briefly, C57BL/6 wild type mice were anesthetized by i.p. injection of ketamine, xylazine, atropine, and saline (100/20/0.4 mg/g body weight), with supplemental doses equal to one fifth of the initial dose administered as required. After anesthesia, the scrotal sac was cut longitudinally and the testis was gently pulled out and cleared of connective tissue to expose the cremaster muscle. Tissue moisture was maintained with warmed sterile Ringer's solution. Next, the muscle flap was opened with a longitudinal incision along the anterior wall of the muscle, taking care to avoid the primary feeding arteriole and venule pair. After incision, the testis was returned to the abdominal cavity and the animal was secured to a heated, costume-designed Plexiglas stage. The muscle flap was then stretched and secured over an imaging window by 30 gauge needles. The stage was then mounted to the microscope. At the end of the experiment, the mouse was euthanized with an overdose of pentobarbital.

Laser Speckle Flowmetry for Imaging of Microvascular Network Flow

When coherent light, such as that from a laser, illuminates a tissue surface, it produces a consistent scatter pattern known as speckle. This pattern is characteristic for a given tissue structure. As elements within the tissue move (i.e. red blood cells) and scatter light differently, the speckle pattern fluctuates. When these fluctuations are integrated over time, such as during the acquisition of a digital image, the image shows a decrease in speckle contrast and variation due to the averaging of the intensity of each speckle. Using spatial statistics of time-integrated speckle contrast, Fercher and Briers (19) showed that this decrease in speckle contrast (C, Eq. 1) can be related to particle flux, where σ is the standard deviation and I is the mean of the pixel (Pij, Fig 1) values in a 7×7 neighborhood. For our calculations, we used a simplified algorithm (Eq. 2) for relating speckle contrast (C) and exposure time (T) to autocorrelation time (τ), which is directly proportional to particle velocity (*SI*, speckle intensity) within the local volume of the optical tissue slice. This simplified algorithm removes the assumption of Gaussian or Lorentzian distributions, and is valid for the flow ranges seen in microvascular networks (e.g dorsal skinfold window chamber) (37).

$$C_{ij}{}^{2}=\frac{\sigma_{ij}^{7\times7^{2}}}{\langle I_{ij}^{7\times7}\rangle^{2}} \quad (1)$$

$$\frac{1}{\tau}=\frac{1}{2TC^2}=LSI \quad (2)$$

In our arrangement, a beam expanded 30mW, 658nm laser diode (Newport LPM658-30) was used to illuminate the window chamber tissue (Fig 1). The raw laser speckle images were collected by an intravital microscope (Zeiss Axioskop, Thornwood, NY) using a 4x air lens (Zeiss Acroplan LD NA=0.1) and acquired and digitized by a cooled, monochrome CCD camera (Optronics Quantifier, Goleta, CA) (7.4 μm × 7.4 μm pixels). The selection of the speckle imaging setup was chosen to balance the resolution of the scope and size of the speckle. During imaging, the speckle of light is projected into the CCD camera at a size (S) of $S=2.44\lambda(1+M)/(2NA)$, where λ, NA, and M are the wavelength of laser light, the numerical aperture of the objective, and the magnification of the objective, respectively. At these settings, the physical size of the CCD pixel element satisfied the Nyquist sampling criteria of at least 2 pixels per individual speckle (25). At each field of view, a sequence of ≥15 12-bit raw speckle images were acquired at variable exposure times to capture average flow. These raw speckle images were converted to laser speckle flow index maps using a MATLAB algorithm. To account for variations in tissue background motion from mouse movement, the processed flow images were normalized to median background intensity and then analyzed using ImageJ software (NIH, Bethesda, MD) to quantify the average speckle flow intensity. Individual network flow images were then merged into larger, 2D microvascular network maps using Adobe Photoshop (CS2, Adobe Systems Inc, San Jose, CA). For dorsal skinfold window chamber microligation experiments, brightfield and processed speckle flow images were merged into separate color panes before montaging, allowing for precise overlay of brightfield and speckle flow network montages.

In Vitro Speckle Tissue Phantom Imaging Protocol

To generate light scattering tissue phantoms, titanium dioxide nanopowder (677469, Sigma Aldrich, St Louis, MO) was sonicated and dispersed into 184 Sylgard PDMS gel (Dow Corning, Midland, MI) at 1mg/mL and allowed to cure overnight. Polyethylene tubing was connected to glass capillary tubes of varying inner diameters and similar wall thicknesses (142, 282, and 447μm, Drummond Microcap, P1799 Sigma Aldrich, St Louis, MO) and placed atop the phantom to mimic a superficial vessel in a scattering tissue medium. The tubing was connected to a PHD2000 syringe pump (Harvard Apparatus, Holliston, MA) which was used to drive a pre-determined, randomized program of flow rates of defibrinated bovine blood (Hemostat Labs, Dixon, CA). Pump rate and image acquisition were controlled by custom-designed LabVIEW software (National Instruments, Austin, TX). Each complete program of flow rates was repeated 5 times at a specific exposure time, hematocrit, or tubing diameter. For hematocrit variation, the defibrinated blood was centrifuged at 800g for 10 min and then resuspended to the initial 36% hematocrit or concentrated by removal of plasma and resuspended to 54% hematocrit. A logarithmically spaced distribution of velocities was used to determine how variation in exposure time (3ms and 20ms) alters the dynamic range of the linear speckle velocity versus absolute velocity relationship.

In Vivo Calibration Imaging Protocol Using Laser Speckle and Microspheres

To determine the relationship between speckle flow measurements and absolute measurements of hemodynamics, circulating fluorescent microspheres were used as tracer particles. Cremaster and window chamber tissues were prepared for intravital imaging, laser speckle flowmetry, and fluorescence microscopy as described above. Both preparations were drip superfused with warmed, sterile Ringer's solution throughout the duration of imaging. A 2% wt/vl green fluorescent microsphere solution (3.0 μm, Fluoro-Max G0300, Thermoscientific, Waltham, MA) was continuously injected intravenously via tail vein catheter at a variable rate (<200 μL/hr) to ensure continuous observation of ≥2 discrete microspheres per frame in the observed microvessels. At least 5 random fields of view per preparation were chosen for imaging. At each field, a 20 second sequence of 100ms exposure images were taken under 100Hz pulsed LED (M455L2-C4, Thorlabs, Newton, NJ) fluorescent epillumination to allow for microsphere tracking. This was immediately followed by the acquisition of a ≥15 frame sequence (4 frames per second) of raw speckle images (<5 seconds switch procedure).

In Vivo Measurement of Altered Network Flow Using Laser Speckle

To determine how arteriole occlusion affects flow throughout large microvascular networks with different degrees of arteriolar interconnectivity, wild-type BALB/c and C57BL/6 mouse strains were implanted with dorsal skinfold window chambers as described above. After 24hrs of post-surgical recovery, mice were induced and maintained under 1.5% inhaled isoflurane anesthesia and prepared for intravital imaging on a warmed microscope stage. After a 15 minute equilibration period, the entire window chamber was imaged by brightfield microscopy and laser speckle flowmetry with the glass coverslips left in place. At each field of view, imaging alternated between brightfield image acquisition using a using 560nm bandpass filter to improve vessel contrast and laser speckle imaging without transillumination or a bandpass filter. A 20ms exposure time was chosen for all imaging steps based on initial experiments. After the initial imaging step, the glass coverslip window was removed and the microcirculation was exposed and drip superfused with warmed, sterile Ringer’s solution. After exposure, the largest feeding arteriole to the window chamber network with adequate separation from its paired venule was chosen for occlusion using a custom designed and fabricated micro-cauterization device capable of isolated cauterization down to an ~100 micron diameter. The tissue was then flushed with sterile Ringer’s solution and a sterile glass coverslip was replaced and secured over the window chamber. Inhaled isofluorane was removed, and the mouse was then allowed to recover for 24 hours. After 24 hours, the mouse was, again, induced and maintained on inhaled isofluorane. After a 15 minute equilibration period, the entire window chamber was reimaged as before with the glass coverslip left in place to generate a second set of brightfield and laser speckle images without a change in laser illumination orientation. Together, these datasets represent the initial hemodynamic state of the window chamber network and the acute (24 hours post-occlusion) hemodynamic state of the entire network in response to the altered network structure and flow patterns induced by the primary feeding arteriole occlusion.

Microsphere Particle Velocity Analysis

To determine hemodynamics using fluorescent microsphere tracer particles, centerline velocity was measured by determining the distance traveled by individual spheres during the observed number of pulsed time steps (10ms at 100Hz LED strobe rate, Fig 3A). Within individual frames, only the fastest moving spheres in the center of the microvessel segment were chosen for analysis to exclude slower microspheres near the vessel wall above and below the central axis that were also visible in the focal plane. A typical sequence of images in a given field of view yielded >3 arteriole or venular segments. Only vessel segments with ≥6 measurable centerline particles during the complete sequence were included in the analysis to ensure an accurate representation of average centerline velocity. While velocity analysis was limited to centerline velocity due to optical clarity and the number of particles visualized during acquisition, centerline velocity represents a useful approximation for mean velocity in microvessels (5, 23).

Laser Speckle Flowmetry Analysis

For individual microvessel segments, average speckle pixel intensity was measured along a length of the given segment across the full diameter of the vessel. A similarly sized region of the neighboring background tissue was also measured for speckle intensity in each field of view or montage separately for each vessel segment. The laser speckle intensity of the vessel (SI_{vessel}) was normalized (NSI, normalized speckle intensity) to the neighboring background intensity ($SI_{background}$) to remove background artifact from general tissue motion and variations in speckle illumination according to Eq 4. With the assumption of Poiseuille flow, wall shear rate is proportional to average blood velocity divided by tube diameter. Therefore, proportional wall shear rate (SSR, speckle shear stress) was calculated using the NSI measurement of average blood velocity and vessel diameter (D) (Eq 4).

$$NSI=\frac{LSI_{vessel}}{LSI_{background}}-1 \quad (3)$$

$$SSR \propto NSI/D \quad (4)$$

Within the cremaster network, individual fields of view containing the input (Q_{parent}) and output ($Q^A_{daughter}$ and $Q^B_{daughter}$) flows at bifurcations were used to assess conservation of mass. To compare NSI and absolute velocity accuracy, relative error from perfect conservation of mass (Eq 5) was calculated from flow estimates for LSF ($Q_{speckle}$) using NSI as a measurement of average velocity (Eq 6) and flow estimates using absolute microsphere centerline velocity (Vc_{sphere}) (Eq 7, assumed Poiseuille flow, where Q_{sphere} is flow).

$$Error(\%)=\frac{\left(Q^A_{daughter}+Q^B_{daughter}\right)-Q_{parent}}{Q_{parent}} * 100 \quad (5)$$

$$Q_{speckle} \propto NSI * D^2\,(a.u.) \quad (6)$$

$$Q_{sphere} \propto Vc_{sphere} * D^2\,(a.u.) \quad (7)$$

Network Structure and Flow Analysis

Using a custom-designed LabVIEW program (available on request), the montaged network images composed of brightfield and speckle velocity data were used to measure diameter and NSI for all arteriole segments in a given window chamber network visible in both the pre-occlusion and post-occlusion microvascular networks. Arteriole segments were defined as the length of vessel between arteriolar branch points. Prior to analysis, all pre- and post-occlusion network pairs were de-identified and randomized. Arcade vessels were defined either as circular, continuous connections of arterioles or venules larger than terminal arterioles or as connections between primary feeding arterioles or draining venules through non-terminal arteriole or venules, respectively. For micro-occlusion experiments to quantify changes in network hemodynamics, individual arteriole segments were classified into “collateral” or “background” in de-identified images. The two most direct and largest continuous diameter arteriole pathways connecting primary feeding arterioles (either self or separate) to the downstream half of the occluded arteriole were termed “collateral” pathways (see Fig 5 for examples). All arteriole branch segments in this pathway were deemed "collateral" segments, all other arterioles in the network that were not designated as "collateral" segments were designated as "background" arteriole segments.

Statistics

For comparison of the distribution of pre-occlusion arteriolar diameter and the percent change in velocity (NSI) and shear rate (SSR) per arteriolar segment (NSI) in BALB/c and C57BL/6 networks, segment diameters and percent change in velocity or shear stress were binned and averaged across all mice within the group. Linearity of the NSI versus known velocity was tested using linear regression. Regression was performed on logarithmically transformed data for in vitro exposure variation analysis using a log distribution of velocity steps. All data were reported with error bars representing ± standard deviation of the mean. Two-way ANOVA statistical testing combined with the Holm-Sidlak method for multiple testing of interactions was used to compare differences in vascular loop structure and change in flow within collateral and background arterioles for BALB/c and C57BL/6 mice. Significance was assessed at $p<0.05$ (Sigma Stat 3.4, Systat Software, San Jose, CA).

Results

In Vitro Testing of Laser Speckle Flowmetry Linear Response

During in vitro tissue phantom testing, the normalized speckle index (NSI) exhibited a highly linear relationship with average blood velocity (>0.97 R^2, Fig 2A, n=6 trials per velocity step at each diameter, 3ms exposure). This linear relationship has no significant variation with diameter spanning from 142 to 447 μm for glass capillary tubes (Fig 2A). Further, this linear relationship has no significant variation with respect to hematocrit when comparing NSI to velocity using 36% PCV and 54% PCV substrate blood (Fig 2B, n=6 trials per velocity step per hematocrit, 3ms exposure). As previously demonstrated (12), altering camera exposure time adjusts the range and sensitivity of the linear operating region of the NSI to velocity relationship (Fig 2C). For a 20ms exposure time, the linear operating range spans from zero to approximately 1mm/s average velocity with sensitivity down to a minimal resolution of 0.05mm/s (0.92 log-weighted R^2 for region to 1mm/s, n=6 trials per velocity step). For a shorter 3ms exposure time, the linear operating range of the NSI to velocity relationship increases, spanning from zero to greater than 20mm/s average velocity. However, sensitivity decreases to a minimal resolution of 0.2mm/s (0.90 log-weighted R^2 for region from 0.2mm/s, n=6 trials per velocity step).

In Vivo Validation of LSF Measurements

Velocity measurements were collected in cremaster and dorsal skinfold window chamber (DSFWC) preparations using circulating fluorescent microspheres and NSI. In the mouse cremaster muscle, a highly linear relationship existed between absolute velocity as measured by fluorescent microspheres and NSI (Fig 3). This linear relationship was true both within a given muscle ($R^2 = 0.66 \pm 0.15$, n=4 cremaster muscles) and across multiple muscles ($R^2 = 0.95$ when binned by 0.1 mm/s increments of absolute velocity, n=4 muscles, Fig 3C). In cremaster muscle, mass balance of flow from parent to daughter vessels was used as an additional verification of accuracy in both particle velocimetry and NSI measurements. NSI measurements showed a similar degree of mass balance error (−6.06 ± 0.04% S.E.M. n=14 bifurcations in n=4 muscles) compared to circulating microsphere measurements (10.03 ± 0.07% S.E.M., no significant differences versus NSI estimates). These similar errors suggest a compounding of error from both NSI and microsphere velocity measurements in the binned data. In the DSFWC, there was a similar degree of linearity of LSI to absolute microsphere velocity measurements within individual preparations ($R^2 = 0.48 \pm 0.16$, n=5 windows) and across preparations ($R^2 = 0.92$, when binned by 0.1 mm/s increments of absolute velocity, n=5 windows, Fig 3E). Interestingly, there was similarity in the NSI versus absolute microsphere velocity slope between cremaster and DSFWC data.

Application of LSF and Brightfield Intravital Imaging to Large Microvascular Networks

As demonstrated in Figure 3D/F, individual fields of view for both brightfield and LSF can be stitched together to yield high resolution maps of vascular structure and blood velocity in both cremaster and DSFWCs. Both cremaster and DSFWC networks demonstrate measurable LSF velocity signal in arterioles <15μm and venules >250 μm in diameter (Fig 3D/F). This resolution allowed for an average of 34.6 arteriole LSF measurable segments per ~80mm^2 of DSFWC tissue. An identical intravital microscopy LSF method was applied to several other intravital preparations including the mouse ear skin and exposed hindlimb skeletal muscle yielding similar results (data not shown).

Alteration in Network and Collateral Pathway Hemodynamics in BALB/c and C57BL/6 Mice

We used a microcauterization device to occlude a primary feeding arteriole in order to determine how the differences in microvascular network structure and function between BALB/c and C57BL/6 mouse strains (Fig 4A/B) alters flow redistribution in response to the loss of a primary feeding arteriole. As previously demonstrated in other organs, C57BL/6 and BALB/c DSFWC microvascular networks showed significant differences between the strains (21, 40, 49). There was a skewing of the BALB/c networks to a higher percentage of small diameter arteriole segments and fewer arteriolar arcade loop structures compared to the C57BL/6 networks (mean pre-ligation arteriole segment diameter; BALB/c = 27.2 ± 7.3μm, n=163 segments in 5 mice: C57BL/6 = 36.8 ± 11.2μm, n=183 segments in 5 mice, Fig 4C/D). However, in converse to the arteriole loops, there was an increase in venular loop structures in the BALB/c networks compared to the C57BL/6 networks (Fig 4D).

Given the significant differences in network structure, we tested whether this would translate into significant hemodynamic differences throughout the network in response to the occlusion of a primary arteriole. LSF was used to quantify hemodynamic changes from pre to 24hrs post primary feeding arteriole occlusion. This was done either independent of network context or with stratification into “collateral” and “background” arteriole segments (Fig 5). When analyzed across an entire network, there were no significant differences in the distribution of velocity or shear stress changes from pre- to post-arteriole occlusion. However, when vessel segments were stratified into likely collateral segments or background arteriole segments, there was a significant percent increase in velocity and shear stress in collateral segments compared to background arterioles ($p<0.023$ and $p<0.045$, respectively, Fig 5B), but this was only significant within the C57BL/6 strain ($p<0.017$ and $p<0.001$, respectively, Fig 5B).

Discussion

Both short and long term autoregulatory responses are the result of the spatial and temporal integration of multiple signals arising from within both the microvascular network and surrounding tissue. In particular, hemodynamic signals are known to be critically important, but they are difficult to characterize in individual microvessels through time. Thus, the ability to obtain hemodynamic information (i.e. velocity, flow, and/or shear stress) on an individual vessel level across entire microvascular networks could represent an important advance in our understanding of integrated “whole-network” microvascular function. However, such measurements are technically challenging due to limitations on resolution, optical clarity, total network area, or duration of experiment. Here, we demonstrate that laser speckle flowmetry is capable of resolving blood velocity across the arteriolar and venular spectrum, on an individual microvessel level, throughout entire microvascular networks.

Further, our data validate that the acquired velocity data from laser speckle imaging is quantitative in nature for blood velocity within and across individual intravital preparations, a question that has been debated previously (17). Of particular interest for the microcirculation, our in vitro testing additionally demonstrates that the laser speckle velocity measurements are independent of vessel diameter and hematocrit, which can vary extensively in the microcirculation (see Fig 4). When taken together, these results indicate that laser speckle flowmetry is a powerful tool for measuring hemodynamics in individual vessels in intact microvascular networks.

Laser Speckle Flowmetry as a Quantitative Tool for Absolute Measurements

The potential ability of LSF to measure absolute velocity is currently under debate (7, 17). Here, our empirical studies suggest that laser speckle can be used to quantitatively determine changes in microvascular velocity and flow at the level of an individual vascular segment. Various laser speckle flowmetry approaches have been used previously for the measurement of hemodynamics in a variety of intravital microscopy models, most prominently in the cerebral circulation (see review (7)), but also in the dorsal skinfold window chamber (12, 37, 47), mesentery (10), and ear circulation (38). However, in contrast to our approach, these studies almost exclusively assessed global or regional changes in tissue perfusion (7), and in vivo validation of laser speckle imaging data was extremely limited. We believe the primary reason for the focus on global and regional perfusion is related to the use of a single “wide field” acquisition to capture the entire network at once. This approach is exemplified in a recent study by Rege et al (38) to equate global and regional alterations in hemodynamics with alterations in vascular structure. Our data on differential C57BL/6 and BALB/c microvascular responses suggest that critically important information can be extracted when hemodynamics are examined on an individual vessel basis.

Advantages of Laser Speckle Imaging

Laser speckle flowmetry applied to intravital microscopy provides several advantages to current techniques available for measuring hemodynamics in the microcirculation. First, LSF has high enough resolution to image individual vessels. This stands in contrast to the bulk perfusion measurements acquired by laser Doppler perfusion imaging (9, 18, 43) and wide field applications of LSF (7, 18, 38). Second, where high resolution is available, such as in the recent development of optical imaging techniques including optical coherent tomography (13, 50), intravital microscopy of fluorescent particles (1, 30, 42), and multiphoton microscopy (24, 26), there are often limitations with respect to spatial coverage and the challenges of registering multiple fields of view. A similar difficulty is present in the more traditional microvascular tools of autocorrelation and dual-slit velocimeters (8, 46) in the experimental duration needed to capture hemodynamics throughout an entire network one vessel at a time. Lastly, LSF is easily integrated into an existing intravital microscopy set up, with low cost and minimal modification. This is in contrast to photoacoustic microscopy, optical coherence tomography, and multiphoton microscopy, which require expensive, uniquely dedicated equipment for data collection and often require extensive custom development (13, 22, 24, 26, 32).

Our results also demonstrate the adaptability of LSF for exploring microvascular network hemodynamics. Specifically, our results on sensitivity and linear dynamic range of LSF demonstrate that variations in camera exposure time can be used to adapt a given LSF setup to the expected velocity range within a specific intravital preparation, as has been suggested previously (12). This would allow for imaging of both low velocity (e.g. in the dorsal skinfold window chamber) and high velocity (e.g. collateral vessel flow in upper hindlimb muscle (data not shown)) intravital preparations. Interestingly, in the two intravital microscopy models of the microcirculation tested here, both setups yielded surprisingly similar in vivo validation relationships. This suggests that LSF should be applicable to a wide variety of intravital preparations and, potentially, there may be a broadly applicable relationship between NSI and absolute velocity across multiple intravital preparations, though this would require additional study. Moreover, although the current study focused on using a spatial algorithm for determining the speckle velocity measurement, it is well documented that the mode of acquisition and speckle algorithm processing can be readily modified to balance for further increases in spatial resolution versus temporal resolution (see review (16)). Though not examined in the current study, further spatial resolution may also be achieved with the use of higher numerical aperture microscope objectives (25), potentially allowing for direct measurement of wall shear rate. Together the adaptable linear range, potentially broad applicability, and ability to readily adjust for increased spatial or temporal resolution demonstrate how LSF can be readily adapted and customized to a large range of microvascular studies on network regulation and hemodynamics.

Use of LSF for Interrogating Network Responsiveness to Microvessel Occlusion in C57BL/6 and BALB/c Mice

In the current study, we sought to demonstrate the power of LSF and individual vessel hemodynamic analysis by examining the responsiveness of two structurally different microvascular networks to primary feeding arteriole occlusion. BALB/c and C57BL/6 mice represent opposite ends of a spectrum of arteriolar connectivity and network structure across inbred mouse strains within the pial (49) and skeletal muscle circulations (21). Here, we demonstrated that similar differences exist for skin microcirculation, as evidenced by the shifted distribution of arteriolar segments within BALB/c windows toward fewer large arteriole segments (Fig 4C), along with a decreased number of anastomotic arcade arterioles (Fig 4D). Interestingly, BALB/c mice exhibited more venular arcade pathways when compared to C57BL/6 mice, an observation not previously reported. While the functional significance of this finding is unknown, a recent study demonstrates that such pathways can have a functional significance in upstream capillary perfusion (31). Together, the data presented here further demonstrate a significant difference in network structure between BALB/c and C57BL/6 mice.

Combining the confirmed difference in network structure between the two strains with the utility of network wide laser speckle flowmetry, we were able to test whether differences in network structure and vasoactivity in C57BL/6 and BALB/c mice create differences in responsiveness to primary arteriole occlusion. Our data show that, when viewed on a network-wide scale, there were few apparent differences in how blood flow is redistributed. This was a somewhat unexpected finding given the well documented differences in perfusion deficits between the two strains upon larger vessel occlusion, such as the femoral artery (21, 40) or middle cerebral artery (49). However, when analyzed on an individual vessel level using network structure as a guide, our data demonstrated that C57BL/6 mice recruit their predicted collateral vessels more efficiently upon primary arteriole occlusion, as denoted by significant increases in velocity and shear stress in collateral segments (Fig 5B). It is important to consider that the observed differential recruitment of collateral arterioles may be a significant factor contributing to the differential capacity to undergo collateral remodeling between the two strains. Though not directly tested, the differences in network structure alone between the two strains may underlie the differential collateral recruitment given that there are no significant differences in conduit artery (39) or arteriolar vasoreactivity (27) between C57BL/6 and BALB/c strains.

While the rules guiding our prediction of collateral arteriole pathways appear successful in identifying “collateral” pathways in the microcirculation upon arteriole occlusion, the complexity of the networks and spread of hemodynamic changes apparent in our network-wide analysis suggest that there were a number of similarly recruited pathways missed by our simple prediction rules. However, even the argument that the observed differences in hemodynamic alterations were related to our ability to predict collateral routes between the networks of the two strains further highlights the necessity for examining hemodynamics across an entire network on an individual arteriole level. To date, the vast majority of studies examining the mechanism of collateral arterial development have focused on networks where it is easy to select for specific vascular segments that undergo reliable hemodynamic changes and/or growth such as the mesentery (20, 45), hindlimb ligation (15, 51), and pial circulation (49). In the microcirculation, the arteriovenous networks are often highly interconnected and variable between individual animals, making examinations of the coordination of hemodynamics and cell signaling mechanisms as related to microvascular remodeling challenging. Further, the inter-individual variations necessitate the use of models that can chronicle these variables over time. Laser speckle flowmetry, therefore, presents a particularly compelling and powerful tool by being able to measure hemodynamics on an individual vessel basis, non-invasively, repeatedly, and without the need of exogenous contrast agents. As such, network-wide LSF can function as a means of stratifying hemodynamic changes across an entire microvascular network that can then be mapped back to the vascular remodeling or cell signaling/recruitment data obtained by other intravital microscopy techniques (Fig 6). Such combinations can pull from the strength of various intravital microcirculation preparations such as the ear (6, 14, 38) which requires minimal surgical intervention or the dorsal skinfold window chamber for understanding of tumor vascularization (41) and vascular remodeling in response to injury/inflammation (33). While the scope of the current study does not cover how network alterations in hemodynamics guide network structural remodeling, the results demonstrate that laser speckle microscope has the potential to explore these questions in conjunction with existing intravital microscopy techniques to begin teasing apart the interplay of hemodynamics in short-term and long-term autoregulation. For example, laser speckle flowmetry could be used to measure the propagation of hemodynamic alterations through a network in response to a localized metabolic or electrical stimulus in order to quantify the relative contribution of circulating and vascular mural connection components to the conducted response of short-term network vasoactivity. Further, the non-invasive nature of laser speckle flowmetry could be combined with transgenic mice with fluorescent markers to understand the temporal recruitment of various immune cell populations driven by hemodynamic changes that guide long-term structural network remodeling.. Taken together, network-wide LSF could be particularly valuable in efficiently acquiring numerous datasets that capture velocity distributions throughout a network during short-term and long-term autoregulation to test and validate some of the autoregulatory insights gained from theoretical modeling (35).

Limitations

Several limitations are necessary to keep in mind when applying LSF to microvascular intravital imaging. First, though our data suggest a potentially broad relationship between speckle flow and absolute flow, this has not been verified in other preparations and the exact relationship may vary if using a different intravital arrangement. Therefore, the measurements from laser speckle are limited to quantifying the relative changes in hemodynamics in individual segments or a distribution throughout a network unless the individual intravital system has been calibrated. Second, there are numerous algorithms for converting raw speckle images to relative velocity. The one chosen in this study is a simplified version to improve processing time and is valid for the longer exposure times required for microcirculation preparations chosen here (37), but it may not be applicable to higher velocities seen in other intravital preparations. Lastly, the network-wide approach generates large quantities of data, which can be difficult to process. However, combinations of manual and semiautomated analysis tools, as in the current study, or automated analysis (38, 47) can be used to aid the process.

Acknowledgments

The authors would like to thank Ji Song for her expertise in cremaster muscle preparation. This work was supported by grants from the National Institutes of Health (R01 HL074082 and R21 HL098632 RJP) and the American Heart Association (10GRNT3490001, RJP). JKM was supported by a pre-doctoral fellowship from the American Heart Association (09PRE2060385) and National Institutes of Health Training grant (T32-HL007284).

Abbreviations

LSF	Laser Speckle Flowmetry
DSFWC	Dorsal Skinfold Window Chamber
SI	Speckle Intensity
NSI	Normalized Speckle Index
SSR	Speckle Shear Rate

References

1. Al-Khazraji BK, Novielli NM, Goldman D, Medeiros PJ, Jackson DN. A simple “streak length method” for quantifying and characterizing red blood cell velocity profiles and blood flow in rat skeletal muscle arterioles. Microcirculation. 2012; 19:327–35. [PubMed: 22284025]
2. Armitage GA, Todd KG, Shuaib A, Winship IR. Laser speckle contrast imaging of collateral blood flow during acute ischemic stroke. J Cereb Blood Flow Metab. 2010; 30:1432–6. [PubMed: 20517321]
3. Ayata C, Dunn AK, Gursoy-OZdemir Y, Huang Z, Boas DA, Moskowitz MA. Laser speckle flowmetry for the study of cerebrovascular physiology in normal and ischemic mouse cortex. J Cereb Blood Flow Metab. 2004; 24:744–55. [PubMed: 15241182]
4. Baez S. An open cremaster muscle preparation for the study of blood vessels by in vivo microscopy. Microvasc Res. 1973; 5:384–94. [PubMed: 4709735]
5. Baker M, Wayland H. On-line volume flow rate and velocity profile measurement for blood in microvessels. Microvascular Research. 1974; 7:131–143. [PubMed: 4821168]
6. Billaud M, Ross JA, Greyson MA, Bruce AC, Seaman SA, Heberlein KR, Han J, Best AK, Peirce SM, Isakson BE. A new method for in vivo visualization of vessel remodeling using a near-infrared dye. Microcirculation. 2011; 18:163–71. [PubMed: 21418375]
7. Boas, Da; Dunn, AK. Laser speckle contrast imaging in biomedical optics. J Biomed Opt. 2010; 15:011109. [PubMed: 20210435]
8. Borders JL, Granger HJ. An optical doppler intravital velocimeter. Microvasc Res. 1984; 27:117–27. [PubMed: 6708823]
9. Chalothorn D, Zhang H, Clayton JA, Thomas SA, Faber JE. Catecholamines augment collateral vessel growth and angiogenesis in hindlimb ischemia. Am J Physiol Heart Circ Physiol. 2005; 289:H947–59. [PubMed: 15833801]
10. Cheng H, Luo Q, Liu Q, Lu Q, Gong H, Zeng S. Laser speckle imaging of blood flow in microcirculation. Phys Med Biol. 2004; 49:1347–57. [PubMed: 15128210]
11. Cheng H, Luo Q, Zeng S, Chen S, Cen J, Gong H. Modified laser speckle imaging method with improved spatial resolution. J Biomed Opt. 2003; 8:559–64. [PubMed: 12880364]
12. Choi B, Ramirez-San-Juan JC, Lotfi J, Stuart Nelson J. Linear response range characterization and in vivo application of laser speckle imaging of blood flow dynamics. J Biomed Opt. 2006; 11:41129.
13. Davis A, Izatt J, Rothenberg F. Quantitative measurement of blood flow dynamics in embryonic vasculature using spectral Doppler velocimetry. Anat Rec (Hoboken). 2009; 292:311–9. [PubMed: 19248163]

14. Demicheva E, Hecker M, Korff T. Stretch-induced activation of the transcription factor activator protein-1 controls monocyte chemoattractant protein-1 expression during arteriogenesis. Circ Res. 2008; 103:477–84. [PubMed: 18669921]
15. Distasi MR, Case J, Ziegler Ma, Dinauer MC, Yoder MC, Haneline LS, Dalsing MC, Miller SJ, Labarrere Ca, Murphy MP, Ingram Da, Unthank JL. Suppressed hindlimb perfusion in Rac2−/− and Nox2−/− mice does not result from impaired collateral growth. Am J Physiol Heart Circ Physiol. 2009; 296:H877–86. [PubMed: 19151256]
16. Draijer M, Hondebrink E, van Leeuwen T, Steenbergen W. Review of laser speckle contrast techniques for visualizing tissue perfusion. Lasers Med Sci. 2009; 24:639–51. [PubMed: 19050826]
17. Duncan DD, Kirkpatrick SJ. Can laser speckle flowmetry be made a quantitative tool? J Opt Soc Am A Opt Image Sci Vis. 2008; 25:2088–94. [PubMed: 18677371]
18. Dunn AK, Bolay H, Moskowitz MA, Boas DA. Dynamic imaging of cerebral blood flow using laser speckle. J Cereb Blood Flow Metab. 2001; 21:195–201. [PubMed: 11295873]
19. Fercher A. Flow visualization by means of single-exposure speckle photography. Optics Communications. 1981; 37:326–330.
20. Van Gieson EJ, Murfee WL, Skalak TC, Price RJ. Enhanced smooth muscle cell coverage of microvessels exposed to increased hemodynamic stresses in vivo. Circ Res. 2003; 92:929–36. [PubMed: 12663481]
21. Helisch A, Wagner S, Khan N, Drinane M, Wolfram S, Heil M, Ziegelhoeffer T, Brandt U, Pearlman JD, Swartz HM, Schaper W. Impact of mouse strain differences in innate hindlimb collateral vasculature. Arterioscler Thromb Vasc Biol. 2006; 26:520–6. [PubMed: 16397137]
22. Hu S, Wang LV. Photoacoustic imaging and characterization of the microvasculature. J Biomed Opt. 2010; 15:011101. [PubMed: 20210427]
23. Ishikawa M, Sekizuka E, Shimizu K, Yamaguchi N, Kawase T. Measurement of RBC velocities in the rat pial arteries with an image-intensified high-speed video camera system. Microvasc Res. 1998; 56:166–72. [PubMed: 9828154]
24. Kamoun WS, Chae S-S, Lacorre DA, Tyrrell JA, Mitre M, Gillissen MA, Fukumura D, Jain RK, Munn LL. Simultaneous measurement of RBC velocity, flux, hematocrit and shear rate in vascular networks. Nat Methods. 2010; 7:655–60. [PubMed: 20581828]
25. Kirkpatrick SJ, Duncan DD, Wells-Gray EM. Detrimental effects of speckle-pixel size matching in laser speckle contrast imaging. Opt Lett. 2008; 33:2886–8. [PubMed: 19079481]
26. Kleinfeld D, Mitra PP, Helmchen F, Denk W. Fluctuations and stimulus-induced changes in blood flow observed in individual capillaries in layers 2 through 4 of rat neocortex. Proc Natl Acad Sci U S A. 1998; 95:15741–6. [PubMed: 9861040]
27. Leonard S, Croy BA, Murrant CL. Arteriolar reactivity in lymphocyte-deficient mice. Am J Physiol Heart Circ Physiol. 2011; 301:H1276–85. [PubMed: 21742997]
28. Meisner JK, Price RJ. Spatial and temporal coordination of bone marrow-derived cell activity during arteriogenesis: regulation of the endogenous response and therapeutic implications. Microcirculation. 2010; 17:583–99. [PubMed: 21044213]
29. Nagahara M, Tamaki Y, Tomidokoro A, Araie M. In vivo measurement of blood velocity in human major retinal vessels using the laser speckle method. Invest Ophthalmol Vis Sci. 2011; 52:87–92. [PubMed: 20702824]
30. Nakano A, Sugii Y, Minamiyama M, Niimi H. Measurement of red cell velocity in microvessels using particle image velocimetry (PIV). Clin Hemorheol Microcirc. 2003; 29:445–55. [PubMed: 14724373]
31. Nguyen J, Nishimura N, Fetcho RN, Iadecola C, Schaffer CB. Occlusion of cortical ascending venules causes blood flow decreases, reversals in flow direction, and vessel dilation in upstream capillaries. J Cereb Blood Flow Metab. 2011; 31:2243–54. [PubMed: 21712834]
32. Nguyen Q-T, Tsai PS, Kleinfeld D. MPScope: a versatile software suite for multiphoton microscopy. J Neurosci Methods. 2006; 156:351–9. [PubMed: 16621010]
33. Nickerson MM, Song J, Meisner JK, Bajikar S, Burke CW, Shuptrine CW, Owens GK, Skalak TC, Price RJ. Bone marrow-derived cell-specific chemokine (C-C motif) receptor-2 expression is

required for arteriolar remodeling. Arterioscler Thromb Vasc Biol. 2009; 29:1794–801. [PubMed: 19734197]

34. Popel AS, Johnson PC. Microcirculation and Hemorheology. Annu Rev Fluid Mech. 2005; 37:43–69. [PubMed: 21151769]
35. Pries AR, Secomb TW. Control of blood vessel structure: insights from theoretical models. Am J Physiol Heart Circ Physiol. 2005; 288:H1010–5. [PubMed: 15706037]
36. Pries AR, Secomb TW. Modeling structural adaptation of microcirculation. Microcirculation. 2008; 15:753–64. [PubMed: 18802843]
37. Ramirez-San-Juan JC, Ramos-García R, Guizar-Iturbide I, Martínez-Niconoff G, Choi B. Impact of velocity distribution assumption on simplified laser speckle imaging equation. Opt Express. 2008; 16:3197–203. [PubMed: 18542407]
38. Rege A, Thakor NV, Rhie K, Pathak AP. In vivo laser speckle imaging reveals microvascular remodeling and hemodynamic changes during wound healing angiogenesis. Angiogenesis. 2012; 15:87–98. [PubMed: 22198198]
39. Ryan MJ, Didion SP, Davis DR, Faraci FM, Sigmund CD. Endothelial dysfunction and blood pressure variability in selected inbred mouse strains. Arterioscler Thromb Vasc Biol. 2002; 22:42–8. [PubMed: 11788459]
40. Scholz D, Ziegelhoeffer T, Helisch A, Wagner S, Friedrich C, Podzuweit T, Schaper W. Contribution of arteriogenesis and angiogenesis to postocclusive hindlimb perfusion in mice. J Mol Cell Cardiol. 2002; 34:775–87. [PubMed: 12099717]
41. Skala MC, Fontanella A, Lan L, Izatt Ja, Dewhirst MW. Longitudinal optical imaging of tumor metabolism and hemodynamics. J Biomed Opt. 2010; 15:011112. [PubMed: 20210438]
42. Smith ML, Long DS, Damiano ER, Ley K. Near-wall micro-PIV reveals a hydrodynamically relevant endothelial surface layer in venules in vivo. Biophys J. 2003; 85:637–45. [PubMed: 12829517]
43. Soehle M, Heimann A, Kempski O. On the number of measurement sites required to assess regional cerebral blood flow by laser-Doppler scanning during cerebral ischemia and reperfusion. J Neurosci Methods. 2001; 110:91–4. [PubMed: 11564528]
44. Strong AJ, Bezzina EL, Anderson PJB, Boutelle MG, Hopwood SE, Dunn AK. Evaluation of laser speckle flowmetry for imaging cortical perfusion in experimental stroke studies: quantitation of perfusion and detection of peri-infarct depolarisations. J Cereb Blood Flow Metab. 2006; 26:645–53. [PubMed: 16251884]
45. Tuttle JL, Nachreiner RD, Bhuller AS, Condict KW, Connors BA, Herring BP, Dalsing MC, Unthank JL. Shear level influences resistance artery remodeling: wall dimensions, cell density, and eNOS expression. Am J Physiol Heart Circ Physiol. 2001; 281:H1380–9. [PubMed: 11514310]
46. Wayland H, Johnson PC. Erythrocyte velocity measurement in microvessels by a two-slit photometric method. J Appl Physiol. 1967; 22:333–7. [PubMed: 6017904]
47. White SM, George SC, Choi B. Automated computation of functional vascular density using laser speckle imaging in a rodent window chamber model. Microvasc Res. 2011; 82:92–5. [PubMed: 21419785]
48. Yang O, Cuccia D, Choi B. Real-time blood flow visualization using the graphics processing unit. J Biomed Opt. 2011; 16:016009. [PubMed: 21280915]
49. Zhang H, Prabhakar P, Sealock R, Faber JE. Wide genetic variation in the native pial collateral circulation is a major determinant of variation in severity of stroke. J Cereb Blood Flow Metab. 2010; 30:923–34. [PubMed: 20125182]
50. Zhao Y, Chen Z, Saxer C, Xiang S, de Boer JF, Nelson JS. Phase-resolved optical coherence tomography and optical Doppler tomography for imaging blood flow in human skin with fast scanning speed and high velocity sensitivity. Opt Lett. 2000; 25:114–6. [PubMed: 18059800]
51. Ziegler, Ma; Distasi, MR.; Bills, RG.; Miller, SJ.; Alloosh, M.; Murphy, MP.; George Akingba, A.; Sturek, M.; Dalsing, MC.; Unthank, JL. Marvels, mysteries, and misconceptions of vascular compensation to peripheral artery occlusion. Microcirculation. 2010; 17:3–20. [PubMed: 20141596]

Perspectives

Here we demonstrated the use of laser speckle flowmetry as a quantitative tool for measuring relative blood velocity and shear stress in large microvascular networks at high resolution. The technique can be easily adapted to a variety of intravital microscopy preparations for examining the microcirculation without the need of exogenous contrast agent. Combining the laser speckle flowmetry technique with the wide array of other methods available to intravital preparations, it will be readily possible to directly examine how changes in hemodynamics coordinate long-term vascular remodeling in microvascular networks and how short-term vasoactivity can modulate network hemodynamics.

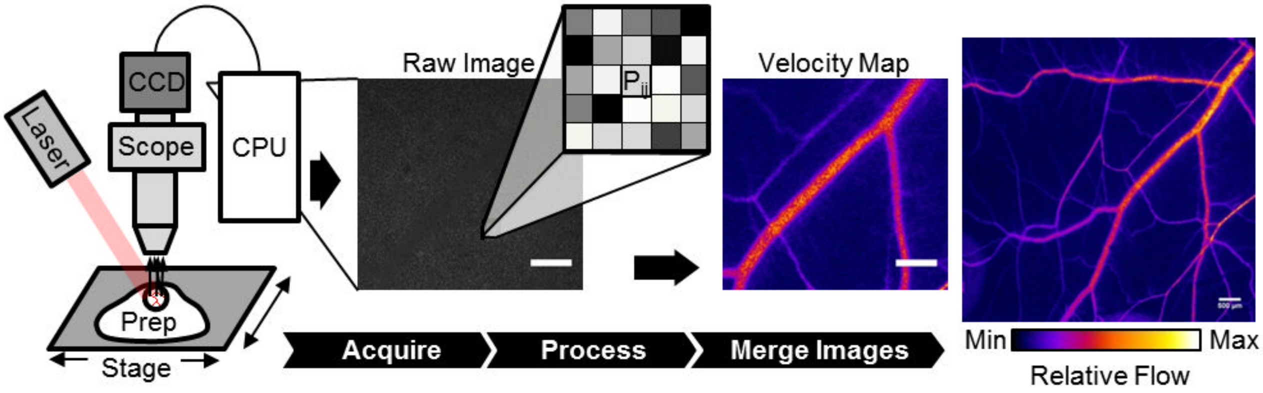

Figure 1. Generation of 2 dimensional blood velocity maps in large microvascular networks

A uniform field of laser light is used to illuminate the intravital tissue preparation. This produces a dynamic speckle pattern that is acquired by a CCD (or CMOS) camera. From the raw digital speckle image, a relative velocity measurement for each pixel (P_{ij}), based on the variance of the speckle pattern in the surrounding 7×7 pixel neighborhood (Eq 1), is used to generate a relative velocity map at the given field of view. For more robust measurements, individual processed speckle images are averaged and then merged into the larger microvascular network (scale bar is 500 μm for all images).

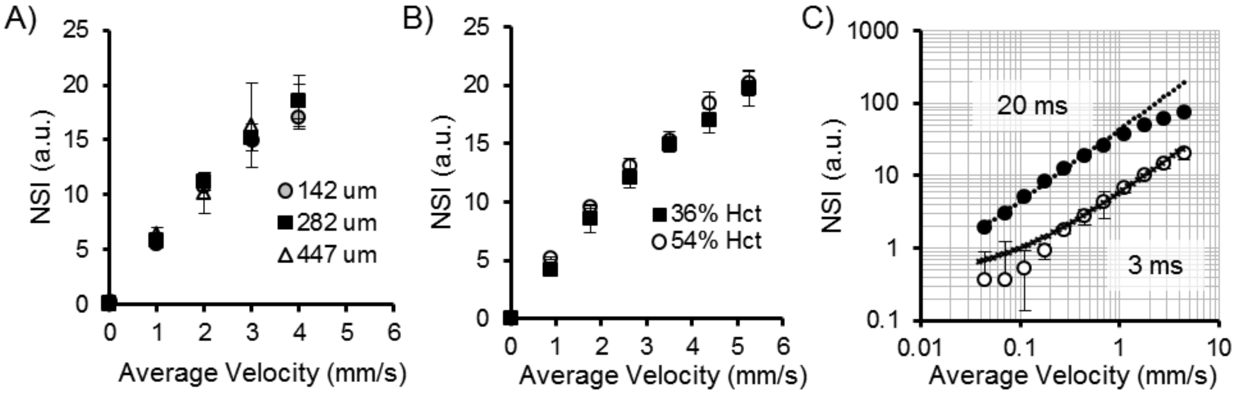

Figure 2. In vitro relationship between normalized speckle index (NSI, arbitrary units, a.u.) and absolute average velocity

A) Glass capillary diameter was increased to approximately 2- (282μm) and 3- (447μm) fold of the initial 142μm diameter with no significant variation in the NSI-velocity relationship (3ms exposure). B) Increasing hematocrit from 36% PCV to 54% PCV demonstrated no significant variation in the NSI-velocity relationship (3ms exposure). C) The linear dynamic range (in log-log scale) of the in vitro NSI-velocity relationship can be shifted by adjusting exposure rate from 3ms exposure (open circles) to 20ms exposure (closed circles). Linear relationship (log-transformed) is displayed with dotted lines (20ms, circles, excludes last 4 non-linear values; 3ms, cross-hatches, excludes first 4 non-linear values).

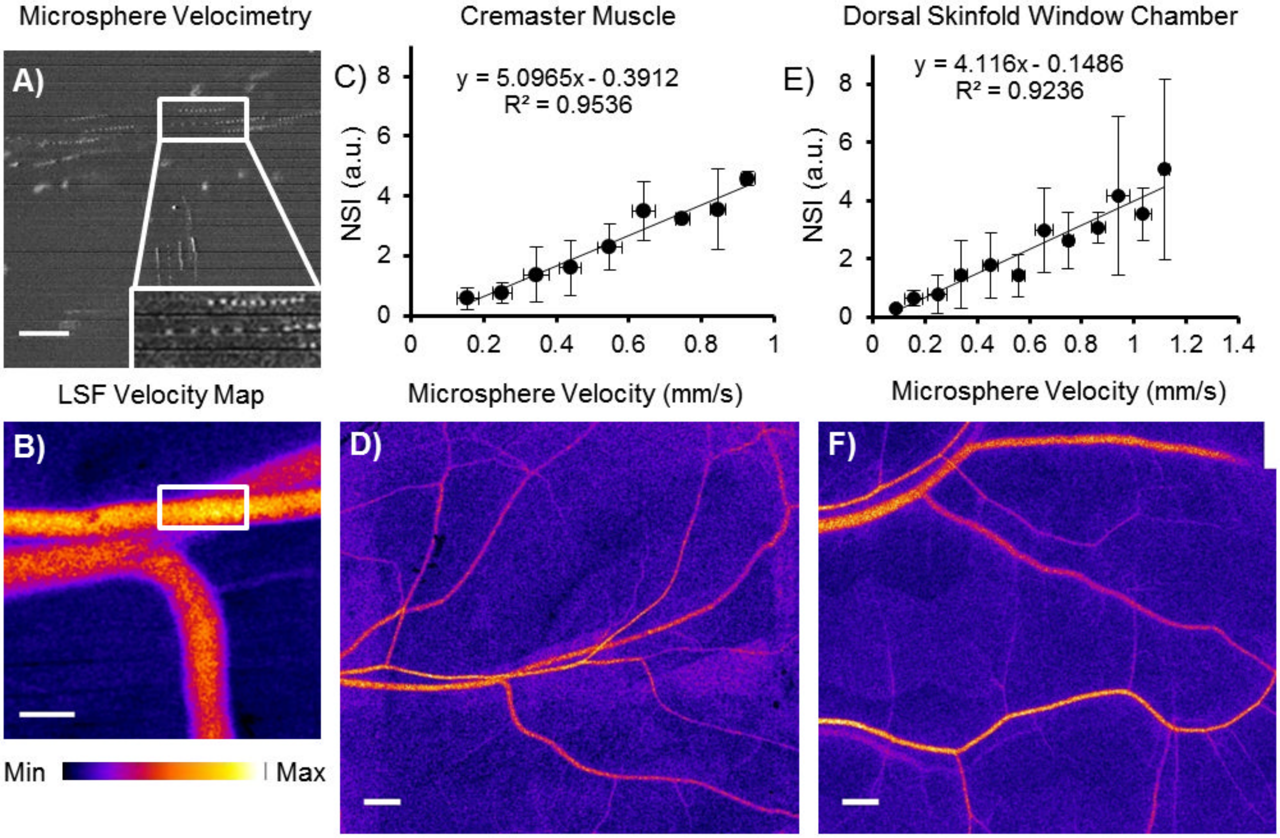

Figure 3. In vivo validation of NSI versus absolute velocity relationship

A) Circulating fluorescent microspheres were used to calculate centerline velocity (pulsed excitation source, 10ms intervals) at each field of view. Inset depicts microsphere traveling in centerline. B) LSF velocity maps were generated for the same field of view immediately after microsphere imaging (scale bar is 100 μm, 3ms exposure). This method was applied in mouse cremaster muscle and dorsal skinfold window chamber. C,E) In vivo relationships between NSI and centerline velocity in the mouse cremaster (C, binned by 0.1mm/s divisions, n=4 muscles) and dorsal skinfold (E, binned by 0.1mm/s divisions, n=5 windows) microcirculation. D,F) Individual fields of view were then merged to form velocity distribution maps of entire microvascular networks (3ms exposure, scale bar is 500 μm).

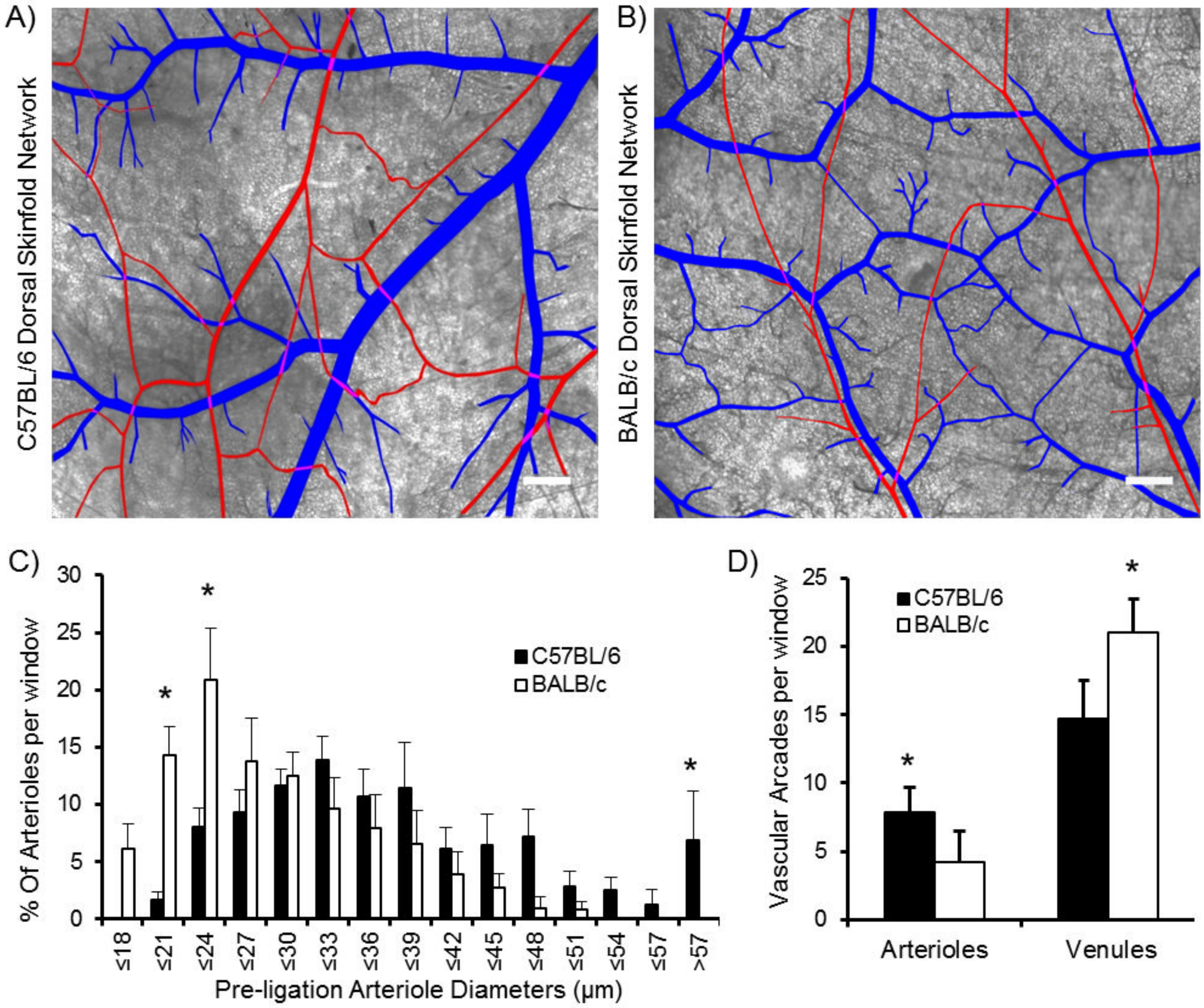

Figure 4. Dorsal skinfold window chamber network structure for C57BL/6 and BALB/c mouse strains

A, B) Demarcated brightfield images of dorsal skinfold window chamber microvascular networks demonstrate differences in network structure between C57BL/6 and BALB/c strains (arterioles in red, venules in blue, scale bar is 500 μm). C) Histogram of pre-ligation arteriole diameters shows skewing of BALB/c segments toward smaller diameters and a significant increase in segments >57 μm in diameter in C57BL/6 networks (* indicates significantly different than other strain within same diameter bin at $p<0.05$, n=5 windows per strain). D) Microvascular arcade loop analysis demonstrates significantly more arteriole loops in C57BL/6 mice, but fewer venular loops compared to BALB/c networks (* indicates significantly different than other strain at $p< 0.05$, n=5 windows per strain).

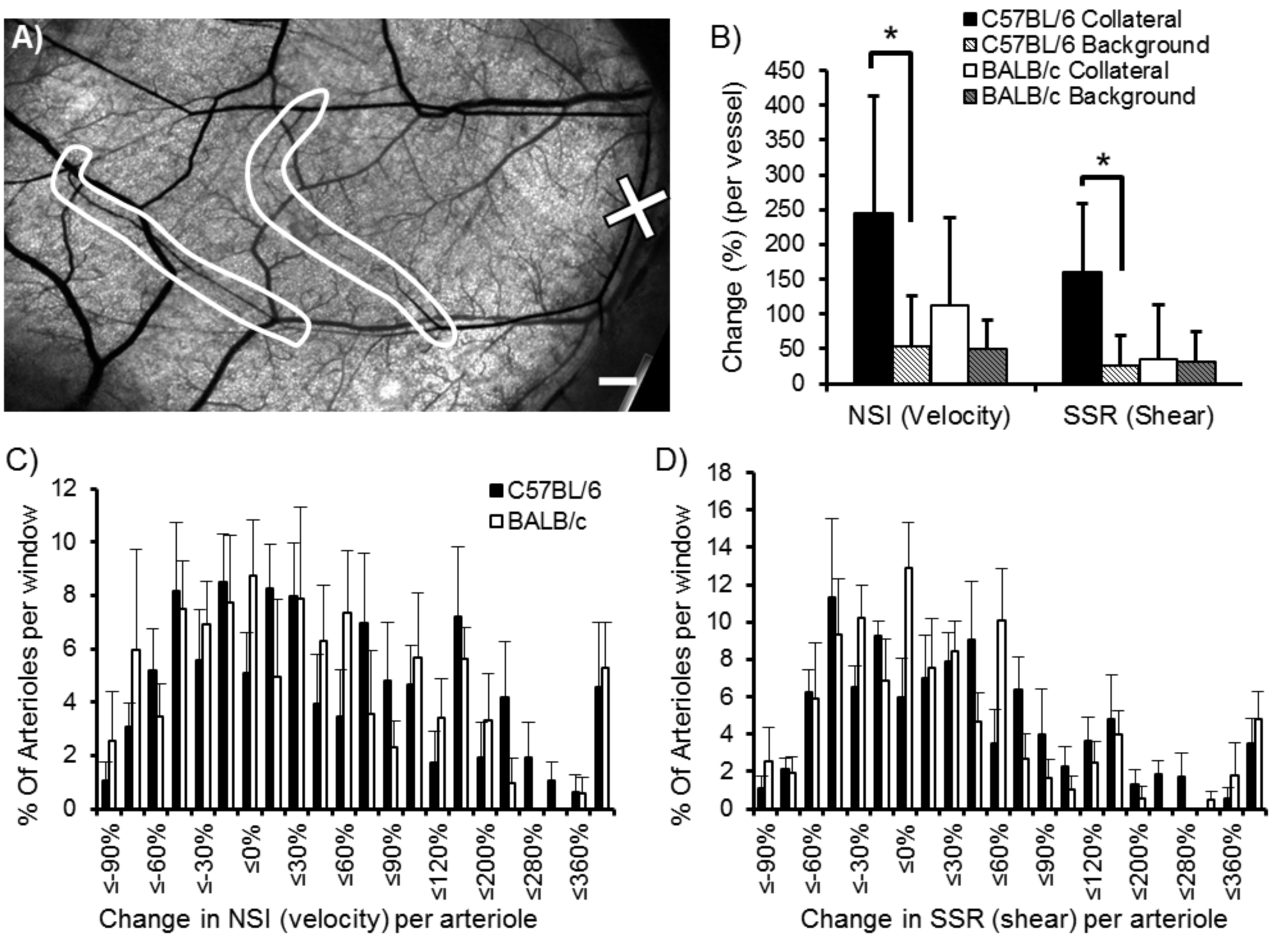

Figure 5. Network hemodynamic alterations after arteriole occlusion in C57BL/6 and BALB/c dorsal skinfold window chambers

A) Representative window chamber network with the chosen site for micro-occlusion (marked by ‘X’) and the predicted collateral pathways (circled in white) (scale bar is 500 μm). B) Bar graph analysis of collateral and background arteriole pathways shows significant increase in collateral velocity and shear stress from pre- to 24 hrs post-microvessel occlusion for the C57BL/6 networks (*, $p<0.05$ between collateral and background changes within strain, n=5 windows per strain). C, D) Histograms representing global analysis of hemodynamic changes (NSI, proportional to velocity, and SSR, proportional to wall shear stress) without stratification. No significant differences were observed between strains (binned by percent change, n=5 windows per strain).

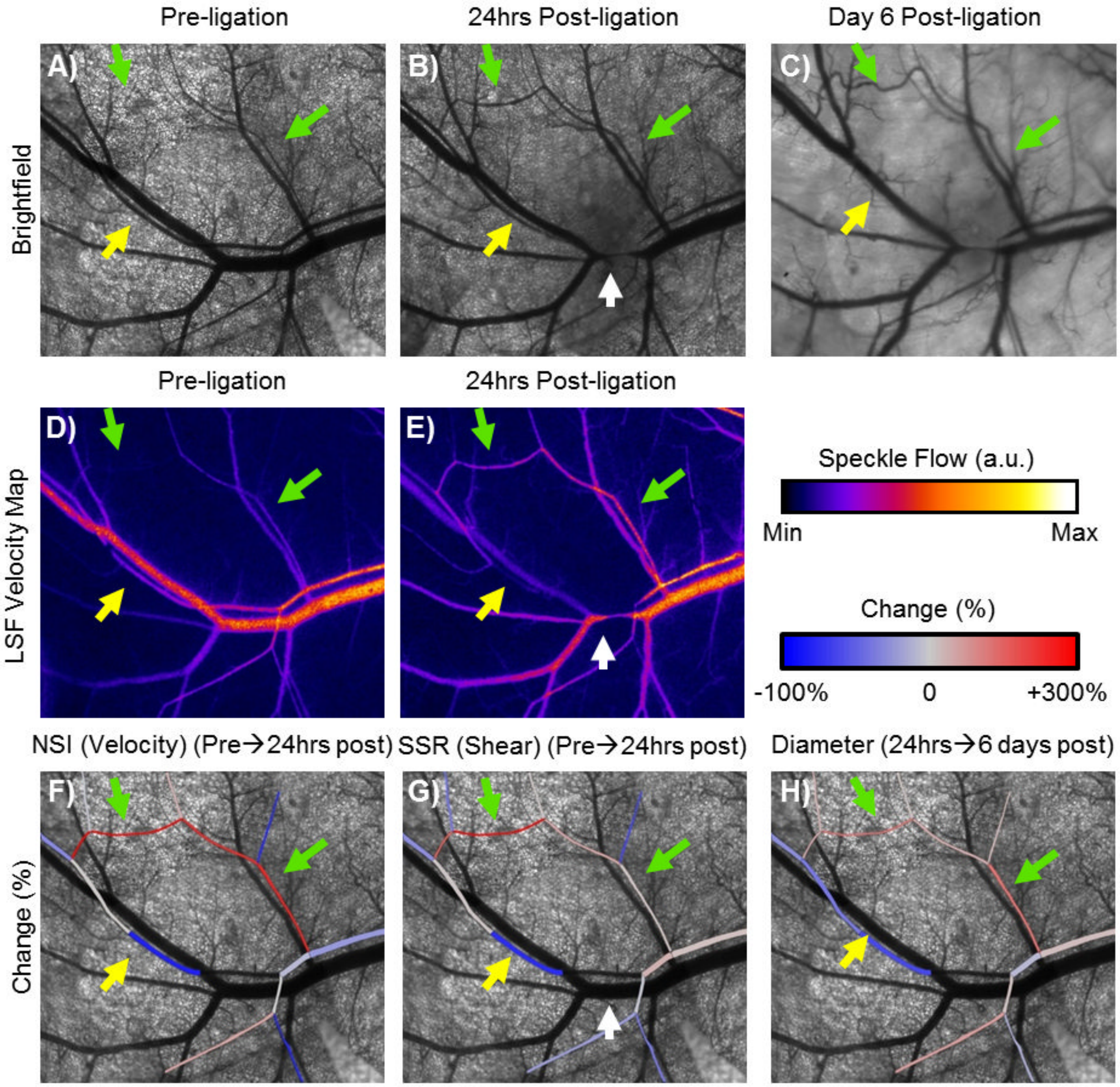

Figure 6. Illustration of how hemodynamic changes and microvascular structure may be mapped in individual microvessels over time using LSF

A–C) Brightfield images of network structure over 6 days after arteriole occlusion in an example window chamber network (green arrows denote collateral pathway exposed to increased velocity, yellow arrow denotes segment exposed to decreased velocity, white arrow indicates site of arteriole occlusion, C57BL/6 strain). Note the increased tortuosity, indicative of outward remodeling, along the high flow pathway. D, E) LSF velocity maps from pre- to 24hrs post-arteriole occlusion. F, G, H) Overlays of changes in velocity, shear stress, and diameter, respectively, on the pre-ligation network demonstrate how changes in hemodynamics using LSF can be mapped back to changes in network structure in a preparation that allows for chronic measurements.